REPOSITORIO UNIVERSIDADE CORUÑA

UNIVERSIDADE DA CORUÑA

This is an ACCEPTED MANUSCRIPT after peer review of the following published document:

A.J. Rodríguez, E. Sanjurjo, R. Pastorino, M.Á. Naya, State, parameter and input observers based on multibody models and Kalman filters for vehicle dynamics, Mechanical Systems and Signal Processing 155 (2021) 107544. https://doi.org/10.1016/j.ymssp.2020.107544

Link to published version:

https://doi.org/10.1016/j.ymssp.2020.107544

General rights:

© 2021. This manuscript version is made available under the CC-BY-NC-ND 4.0 license https://creativecommons.org/licenses/by-nc-nd/4.0/

State, parameter and input observers based on multibody models and Kalman filters for vehicle dynamics

Antonio J. Rodríguez [a] [1], Emilio Sanjurjo[a], Roland Pastorino[b], Miguel Ángel Naya[a]

[a] *Mechanical Engineering Laboratory, University of A Coruña, Escuela Politécnica Superior, Mendizábal s/n, Ferrol 15403, Spain*
[b] *Test Division, Siemens Digital Industries Software, Interleuvenlaan 68, B-3001 Leuven, Belgium*

Abstract

The aim of this work is to present a novel accurate estimator for vehicle dynamics. Following the multibody dynamics approach, a vehicle can be modeled with a high level of detail including non-linear dynamics. As a consequence, a rich simulation data-set is available for engineering analysis, richer than with vehicle analytical models.

The proposed novel estimator is a new form of a dual Kalman filter. The first filter uses an indirect extended Kalman filter (i.e. the errorEKF) incorporating force estimation and using a vehicle multibody model. The second filter is an unscented Kalman filter (UKF) used to increase the accuracy of the errorEKF by estimating uncertain modeling parameters such as the mass of the vehicle and the tire-road friction coefficient.

The performance of the proposed state-parameter-input (SPI) observer is tested in a simulation environment. The performance of the observer is demonstrated using two maneuvers, out of which one covers aggressive driving conditions. The results show that the new observer estimates with high accuracy the variables of interest for vehicle dynamics, such as the tire forces.

Keywords: Multibody dynamics, Kalman filter, State observer, Force estimation, Parameter estimation, Digital twin, Virtual sensing, Vehicle dynamics, tire-road friction coefficient

1. Introduction

Road traffic safety is a major concern worldwide, since it is the 8$^{\text{th}}$ cause of mortality, and the first one in children and young adults from 5 to 29 years [1]. Therefore, driving aids are gaining popularity, with the ABS and the electronic stability program (ESP) present in all the automobiles sold in the United States

[1] Corresponding author, antonio.rodriguez.gonzalez@udc.es

of America and in Europe. More advanced driving aids are quickly gaining popularity in the last years, such as the lane keeping aid, or the collision avoidance system.

All these driving aids require precise and timely information of the vehicle. While current vehicles are equipped with many sensors, there are still some magnitudes that cannot be measured directly due to technical or economical reasons. As an alternative, the estimation of those quantities, also known as virtual sensing, is proposed. Some of the most challenging problems are the determination of the tire forces, the tire-road friction coefficient, and the navigation problems, especially when a GPS signal is not available due to temporary lack of sky visibility (tunnels, high trees, urban canyon, etc.). There are plenty of works in recent years seeking to provide more reliable estimations of these magnitudes or related parameters, in particular those ones focused on achieving these estimations without using additional sensors with respect to a commercial vehicle, or with few additions. In [2], a neuro-fuzzy ANFIS algorithm is combined with an unscented Kalman filter to estimate the slip angle of a vehicle. An extended Kalman filter is presented in [3] to estimate the mass of a vehicle. In [4], a dual Kalman filter is employed to estimate both vehicle mass and road profile. Another approach is presented in [5], where an Extended Kalman filter is used to estimate tire forces, road grade, and road bank angle. In this latter work, an artificial neural network is employed instead of a tire model.

Most of the research made in state estimation relies on analytical models. They are commonly used in control applications, due to their simplicity and low computational cost. This allows to achieve real-time performance, required in most automotive applications. Each analytical model is developed for an specific use-case. The vehicle model is simplified neglecting the dynamic effects that do not have a strong influence in the variables which are estimated.

In other fields of the automotive industry, multibody models are widely used. Such is the case of vehicle design, where multibody models are employed in a simulation environment in order to optimize the vehicle. Through a multibody approach, the same model can describe with fidelity the dynamic behaviour of a vehicle in any situation. The use of these models can be extended to the next steps of the development phase and life cycle of the vehicle, combining the multibody model with a state estimator. The multibody model could be employed as a digital-twin of the real vehicle for control purposes, vehicle testing or durability analysis.

Developing a multibody model of a vehicle requires more effort than an analytical model and, if there is no access to accurate information of the vehicle, it might not be worth it. However, if available, the multibody model can be used for state estimation, enriching the data-set that can be obtained through virtual sensors based on a unique vehicle model. The main disadvantage of using a multibody model is related with its high computational cost. However, this issue is being addressed in different works, as in [6].

The application of multibody dynamics for state estimation was first studied in [7]. Due to the non-linear nature of multibody models [8], the equations of the multibody dynamics were combined with an extended Kalman filter (EKF).

Later, in [9], this approach was applied to a multibody model of an automobile. However, this method entails high computational cost. In [10], the complexity of the implementation was reduced with the use of an unscented Kalman filter (UKF). With this approach, the computational cost is even higher for systems such as an automobile.

In [11] an efficient state estimator for multibody models was presented. It is referred to as errorEKF. This formulation improves significantly the computational cost of previous approaches when applied to an automobile, achieving real-time performance in a conventional personal computer (PC). The development of this new filter continues in [12] and [13], where the input force estimation is included in the filter. Although this method shows promising results when applied to a planar mechanism, it should be evaluated with a multibody model of an automobile. The force estimation based on multibody models was also studied in [14]. Two partially coupled observers are designed to estimate the kinematics and dynamics of the system. The method has been applied to a hydraulic excavator in [15]. Although the method shows accurate results, it is required to measure the acceleration of each degree of freedom of the system.

When modeling a vehicle, a large amount of parameters is involved. Most of those parameters, such as the geometry of the suspension system, remain constant during the life cycle of the vehicle. Meanwhile, the inertial properties of the vehicle, such as the mass, can vary depending on the number of passengers or luggage [16] and the tire-road coefficient can be affected by meteorological conditions or tire wear. Both parameters play an important role on vehicle dynamics, affecting the acceleration, braking, handling and comfort [3].

As stated in [16, 17, 3, 4], combining state and parameter estimation can improve the quality of the estimations. The state estimation is combined with parameter estimation in the so-called Dual Kalman Filters, where two different filters work in parallel. In [16, 4], the mass estimation is used to improve the state estimations, yielding to more accurate results. In [17], the road friction coefficient is estimated together with the states, and shows the benefits of combining the parameter and state estimation in a maneuver with changes in the road friction coefficient.

In this research, the errorEKF with force estimation is combined with a parameter estimator. Due to the uncertainties presented in parameters such as the mass and tire-road friction coefficient, complementing the errorEKF with a parameter estimator increases the accuracy of the estimations.

2. Methodology

The state-parameter-input observer presented in this work makes use of the multibody model of the vehicle presented in Figure 1. It is a rear-wheel drive electric vehicle instrumented with a variety of sensors, summarized in Table 1. Furthermore, there is also information regarding the steering wheel angle and engine torque in order to mimic the driver actions.

The observer is designed in a simulation environment in order to perform simulation batches to research its performance and characteristics. Working in a



Fig. 1 Modeled vehicle

Table 1 Characteristics of the considered sensors

Sensor	Frequency (Hz)	Noise
GPS XY position	5	1.785
GPS Z position	5	2.3
GPS Speed	5	0.053
Accelerometer	250	0.447
Gyroscope	250	0.011
Susp. displ.	250	0.01
Wheel angle	250	0.078

simulation framework allows avoiding long development time and costs. In this virtual framework, three multibody models are employed. They are detailed hereafter.

The first model represents the physical prototype of the vehicle. It is referred during this work as *real vehicle* and it is used as the *ground truth*. The sensors included in the model are the same as the sensors installed in the physical prototype. The sensor data is extracted from the kinematics of this model. White noise is added to represent the noise properties of real sensors.

The second model represents the *model* of the *real vehicle*, which is subject to modeling uncertainties. When building a multibody model, usually the geometry can be accurately determined, but the force models have much more uncertainty. Since this work is developed in a simulation environment, errors in the force models are introduced. This creates a behavior discrepancy (also called model drift) between the *real vehicle* and its *model* similar to the drift existing in a real application. In this work, known errors in the vehicle mass and tire-road friction coefficient are introduced. As stated in Section 1, both parameters have a strong influence on the vehicle dynamics. Since they are also parameters commonly fluctuating during driving, it is important to estimate their real value.

The third model is the one that will be used by the estimator. It will be named *observer* in this work. The multibody model used for the *observer* is

the same as the *model*, except for its parameters. Since it is combined with the state-parameter-input observer, the errors are corrected with the information provided by the sensors installed on the *real vehicle*.

3. Vehicle modeling

Prior to present the observer developed in this work, it is necessary to introduce the particularities of the modeling phase, as they are relevant for the observer design. On the one hand, the multibody coordinates and formulation selected can affect to the integration with the estimator. On the other hand, in vehicle dynamics, the tire model is important when it comes to represent the vehicle dynamics in a reliable form. Next sections are focused on both aspects of the vehicle modeling.

3.1. Multibody dynamics

Since this work is focused on real-time automotive applications, the formulation presented in [18] is employed. In this work, Cuadrado *et al.* present a novel multibody modeling approach for real-time automotive applications. The vehicle model is designed in relative independent coordinates (one coordinate per degree-of-freedom), leading to a multibody system of a minimum size and avoiding the definition of constraint equations. The computational cost of the multibody system is, therefore, quite reduced.

The chassis is modeled with three Cartesian Coordinates ($x\ y\ z$) representing its translation, and three Cardan angles to describe the orientation of the chassis ($\alpha\ \beta\ \gamma$).

Each suspension system is modeled with one coordinate associated to the vertical suspension deflection, $\bar{z}_i$. Normally, the complex kinematic behavior of a suspension system would imply more than one coordinate. However, as in [18], the suspension system is replaced by look-up tables, where the kinematics of the knuckle are derived as a function of $\bar{z}_i$. It must be noted that, since the front suspension depends on the steering input, a different look-up table of the front suspension for each value of the steering input has been generated. Terms due to the variation in time of the steering input have been neglected in the calculation of the velocities and accelerations of the front knuckles [18].

Finally, the wheels are modeled through a revolute joint representing the rotation axis around the knuckle ($\varphi_1\ \varphi_2\ \varphi_3\ \varphi_4$).

The coordinates employed are grouped into vector z. The steering angle is not considered as a variable, since it is an input to the model and not a coordinate itself. Thus, the model has a total of fourteen relative independent coordinates.

$$\mathbf{z} = \left[\begin{array}{cccccccccccccc} x & y & z & \alpha & \beta & \gamma & \bar{z}_1 & \bar{z}_2 & \bar{z}_2 & \bar{z}_4 & \varphi_1 & \varphi_2 & \varphi_3 & \varphi_4 \end{array}\right] \quad (1)$$

The dynamics of the vehicle are derived through the semi-recursive formulation presented in [19]. Since the detailed explanation of the multibody formulation employed is out of the scope of this work, it is briefly described hereafter. The reader is referred to [19, 20, 21] for further details.

Due to the modeling in independent coordinates, the equations of motion (Equation 2) are a set of ordinary differential equations (ODEs), instead of the differential-algebraic system of equations (DAEs) typically obtained in multi-body dynamics,

$$\mathbf{M}\ddot{\mathbf{z}} = \mathbf{Q} \tag{2}$$

where $\mathbf{M}$ and $\mathbf{Q}$ are the mass matrix and force vector of the system. Both the mass matrix and the force vector can be expressed with respect to the relative coordinates (Equation 1) via their intermediate expression with respect to a newly defined set of coordinates $\mathbf{Z}$,

$$\mathbf{Z} = \begin{bmatrix} \dot{s} \\ \omega \end{bmatrix} \tag{3}$$

where $\dot{s}$ is the velocity of the point of the body which is coincident with the fixed frame origin in a particular time step, thus representing the translations of the body, and ω is the angular velocity of the body, which represents the rotations of the body.

These coordinates, called body coordinates, can be related with the set of relative coordinates through the kinematic relations of two neighbor bodies, denoted by *i-1* and *i*,

$$\mathbf{Z}_i = \mathbf{Z}_{i-1} + \mathbf{b}_i\dot{\mathbf{z}}_i \tag{4}$$

$$\dot{\mathbf{Z}}_i = \dot{\mathbf{Z}}_{i-1} + \mathbf{b}_i\ddot{\mathbf{z}}_i + \mathbf{d}_i \tag{5}$$

where the form of terms b_i and d_i varies depending on the type of joint connecting the bodies *i-1* and *i*. They can be obtained following the procedure presented in [20]. As an example, if they are derived for the case of a revolute joint, the following expressions are obtained,

$$b_i = \begin{bmatrix} \tilde{r}_i u_i \\ u_i \end{bmatrix} \tag{6}$$

$$d_i = \begin{bmatrix} \tilde{r}_i(\tilde{\omega}_{i-1}u_i)\dot{z}_i + (\tilde{\omega}_{i-1}\tilde{\omega}_{i-1} - \tilde{\omega}_i\tilde{\omega}_i)\tilde{r}_i \\ \tilde{\omega}_{i-1}u_i\dot{z}_i \end{bmatrix} \tag{7}$$

where r_i is the position of the joint, u_i is the unit vector which defines the direction of the joint, and $\tilde{}$ indicates that each vector is expressed in the form of its skew-symmetric matrix.

Through the recursive procedure presented in [19], the transformation matrix, $\mathbf{R}$, can be defined in such a way that,

$$\mathbf{Z} = \mathbf{R}\dot{\mathbf{z}} \tag{8}$$

$$\dot{\mathbf{Z}} = \mathbf{R}\ddot{\mathbf{z}} + \dot{\mathbf{R}}\dot{\mathbf{z}} \tag{9}$$

Applying the transformation matrix, the mass matrix, $\bar{\mathbf{M}}$, and force vector, $\bar{\mathbf{Q}}$, defined in body coordinates can be converted into their respective expressions in relative coordinates due to Equations 10 and 11 respectively.

$$\mathbf{M} = \mathbf{R}^{\mathrm{T}}\bar{\mathbf{M}}\mathbf{R} \tag{10}$$

$$\mathbf{Q} = \mathbf{R}^{\mathrm{T}}(\bar{\mathbf{Q}} - \bar{\mathbf{M}}\dot{\mathbf{R}}\dot{\mathbf{z}}) \tag{11}$$

3.2. Tire model

Vehicle dynamics is highly influenced by the interaction tire-road [22] and, thus, an accurate tire model should be employed. Although complex tire models, such as the ones based on finite-elements, represent the tire behavior with high fidelity, they are computationally extensive. As an alternative, tire models based on empirical data combined with equations representing the physical behavior of the tire are used.

Normal force tire behavior can be considered similar to a spring-damper system [23]. However, the horizontal dynamics is more complex. In [24], the TMeasy is presented as an empirical-physical tire model for low frequency applications in vehicle dynamics. The number of required parameters is reduced according to the limited availability and accuracy of the basic experimental data. With respect to the tire dynamics, it includes first order dynamics for the longitudinal and lateral tire forces [24]. Hence,

$$\underbrace{F_x(v_x + \dot{\xi}_x)}_{F_x^D} \approx \underbrace{F_x(v_x)}_{F_x^S} + \frac{\partial F_x}{\partial v_x}\dot{\xi}_x \tag{12}$$

$$\underbrace{F_y(v_y + \dot{\xi}_y)}_{F_y^D} \approx \underbrace{F_y(v_y)}_{F_y^S} + \frac{\partial F_y}{\partial v_y}\dot{\xi}_y \tag{13}$$

where v_x and v_y are the longitudinal and lateral velocities of the contact point, F_x^D and F_y^D are the dynamic tire forces, F_x^S and F_y^S are the steady-state tire forces, and $\dot{\xi}$ is the velocity of the tire deflection.

For obtaining the lateral and longitudinal deformation, in [24], the first order equations of the tire dynamics, 12 and 13, can be related with the expressions for the tire forces if the tire is considered as a spring-damper element,

$$F_x^D = k_x\xi_x + c_x\dot{\xi}_x \tag{14}$$

$$F_y^D = k_y\xi_y + c_y\dot{\xi}_y \tag{15}$$

$$F_z^D = k_z\xi_z + c_z\dot{\xi}_z \tag{16}$$

where k and c are the stiffness and damping coefficients of the tire on each direction respectively, $\mathbf{F}$ are the tire forces and ξ is the tire deflection, which

should be determined. Hence,

$$\left(v_x^* d_x + \frac{\partial F_x^S}{\partial s_x}\right)\dot{\xi}_x = -\frac{F}{s_g}(v_x - r_D\Omega) - v_x^* c_x \xi_x \tag{17}$$

$$\left(v_y^* d_y + \frac{\partial F_y^S}{\partial s_y}\right)\dot{\xi}_y = -\frac{F}{s_g} v_y - v_y^* c_y \xi_y \tag{18}$$

where Ω is the angular velocity of the wheel, $v_x^* = r_D|\Omega|\hat{s}_x + v_n$, $v_y^* = r_D|\Omega|\hat{s}_y + v_n$, s_x and s_y are the slip in each direction and s_g the generalized slip (which expressions are in [24]), and F is the total tangential force provided by the tire, which can be obtained through tire characterization as function of the slip. The longitudinal and lateral deflections are obtained through the integration of the differential Equations 17 and 18 each time step [11].

The normal deflection, ξ_z, is obtained through the difference between the unloaded wheel radius and the real distance from the wheel center to the ground. Its velocity, $\dot{\xi}_z$, can also be derived from the relative movement of the contact point towards the wheel center. The force obtained is later restricted in such a way that it can only produce compression forces over the road.

Finally, once the tire deflections are calculated, the tire forces are obtained through Equations 14 to 16. The tire torques are then calculated as the torque produced by the tire forces in the wheel center.

4. Design of the State-Paramater-Input Observer

The presented state observer is meant to be used in real-time applications. Hence, the efficiency of the implementation is a determinant factor. In this work, two different Kalman filters have been combined: the extended Kalman filter (EKF) and the unscented Kalman filter (UKF). While the EKF is employed to estimate the states and inputs of the multibody model, the UKF is in charge of parameter estimation.

The EKF has been widely used for state estimation in vehicle dynamics applications. It is a Kalman filter that can be applied to non-linear systems such as multibody models. The EKF is based on the linearization of the model functions through the Jacobian matrix which relates the states and the model variables. One of the major advantages of this kind of filter is its high computational efficiency. This is a key factor considering that achieving real-time performance is desirable for most vehicle dynamics applications. As stated in [10, 12], it greatly overcomes the UKF in terms of computational cost when applied to multibody models. As presented in [7, 9], combining an EKF with a multibody model can be challenging. In [12], different filters from the EKF family are compared when applied to multibody models. From the results, an indirect filter known as errorEKF shows advantages regarding both easiness of implementation and computational cost.

With respect to parameter estimation, using an EKF approach implies to determine the relation between the model variables and the parameters. For

some parameters, this relation is complex to obtain. As an alternative, the UKF can be used for parameter estimation. In the UKF, the statistical properties of the estimation are propagated through a set of deterministically chosen samples. This reduces the complexity of the implementation [12] while keeping similar results [25], at the cost of a higher computational cost, which grows with the number of states. Hence, only the most relevant parameters should be estimated.

Following the work of Sanjurjo et al. in [13], different versions of the errorEKF have been developed. From them, the errorEKF with force estimation shows higher accuracy due to the input estimation. Thus, it is selected to estimate the states and input forces of the vehicle. When applied to a multibody vehicle model, although the states are estimated with high accuracy, the corrections are not sufficient to properly estimate the tire forces. This behavior is especially noticeable when the errors between the model and the reference appear in the mass or friction coefficient. Since force measurements are not employed in this work, noticeable errors in the mass matrix would lead to biased force estimations [13], because the force estimation relies on the mass matrix and the acceleration error (Section 4.2). Errors due to badly characterized tire-road friction severely degrade the accuracy of the multibody model predictions used as the plant of the Kalman filter. Furthermore, the uncertainties on both variables are high: the mass varies due to several factors (number of passengers, fuel volume, etc.) and the friction coefficient depends on the road, tires, and meteorological conditions. The observer is described in the diagram of Figure 2.

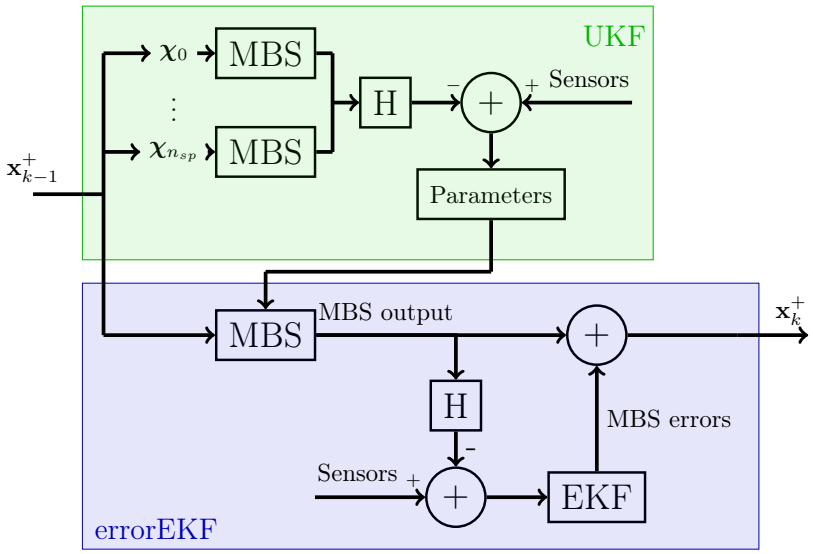


Fig. 2 Simplified flow diagram of a time step of the state-parameter-input observer designed.

In a first step, the parameters are estimated through the UKF approach.

After that, the errorEKF performs the state and input estimation based on a multibody model whose parameters have been updated with the estimations of the UKF.

4.1. UKF for parameter estimation

The UKF is a filter from the family of the sigma-point Kalman filters (SPKFs). The estimations of this kind of filters are made through a set of deterministically chosen weighted sample points [10]. Each sample point, called *sigma-point*, is propagated through the dynamic functions of the multibody model to obtain the observations. The ensemble mean and covariance of the derived observations give a good estimate of the true mean and covariance [26].

The first step in the UKF is to calculate the set of sigma-points, which are a total of $n_{sp} = 2L + 1$, being L the dimension of the state vector. The sigma-points are obtained following Equation 19.

$$\boldsymbol{\chi}_k(i) = \begin{cases} \hat{\mathbf{x}}_k & i = 0 \\ \hat{\mathbf{x}}_k + \gamma(\sqrt{\mathbf{P}_k})_i & i = 1, ..., L \\ \hat{\mathbf{x}}_k - \gamma(\sqrt{\mathbf{P}_k})_i & i = L+1, ..., 2L \end{cases} \tag{19}$$

where $\boldsymbol{\chi}_k(i)$ is the $i-th$ sigma-point, $\mathbf{P}_k$ is the covariance matrix of the system, $\gamma = \sqrt{L + \lambda}$, $\lambda = \alpha^2(L + \kappa)$, α and κ are user-defined tuning parameters, $\sqrt{}$ is the matrix square-root using lower triangular Cholesky decomposition and $()_i$ represents the $i - th$ column [10, 27].

Prior to start with the propagation of the sigma-points, the state vector of the filter must be defined. As stated above, the parameters to estimate are the suspended mass, m, and the tire-road friction coefficient, μ. Thus, the state vector is as shown in Equation 20.

$$\mathbf{x}_k = \begin{bmatrix} m \\ \mu \end{bmatrix} \tag{20}$$

Starting from an estimated mean and covariance over the state vector, five sigma-points are derived. Thus, for a time step k, the *a priori* state estimates and the covariance matrix can be derived from the weighted mean and covariances of the sigma-points, as is expressed in Equations 21 and 22.

$$\hat{\mathbf{x}}_k^- = \sum_{i=0}^{n_{sp}-1} w_i^m \boldsymbol{\chi}_k^-(i) \tag{21}$$

$$\mathbf{P}_k^- = \sum_{i=0}^{n_{sp}-1} w_i^c (\boldsymbol{\chi}_k^-(i) - \hat{\mathbf{x}}_k^-)(\boldsymbol{\chi}_k^-(i) - \hat{\mathbf{x}}_k^-)^{\mathrm{T}} + \boldsymbol{\Sigma}_k^P \tag{22}$$

being $w_0^m = \lambda/(L + \lambda)$ and $w_0^c = w_0^m + (1 - \alpha^2 + \beta)$, $w_i^c = w_i^m = 1/[2(L + \lambda)]$ for $i = 1, ..., n_{sp} - 1$ and β a scaling factor used to control the weighting of the zeroth sigma-point. $\boldsymbol{\Sigma}_k^P$ represents the covariance matrix of the plant noise.

For obtaining the Kalman gain in order to estimate the *a posteriori* state vector, the sigma-points are propagated executing as many multibody simulations as sigma-points for the time step k. The observations (i.e simulated sensor measurements) of each simulation are weighted and added as stated in Equation 23 to obtain the Kalman gain.

$$.\mathbf{K}_k = \mathbf{P}_{x_k y_k} \mathbf{P}_{y_k y_k}^{-1} \tag{23}$$

$$\mathbf{P}_{x_k y_k} = \sum_{i=0}^{n_{sp}-1} w_i^c (\boldsymbol{\chi}_k^-(i) - \hat{\mathbf{x}}_k^-)(\mathcal{Y}_k^-(i) - \hat{\mathbf{y}}_k^-)^{\mathrm{T}} \tag{24}$$

$$\mathbf{P}_{y_k y_k} = \sum_{i=0}^{n_{sp}-1} w_i^c (\mathcal{Y}_k^-(i) - \hat{\mathbf{y}}_k^-)(\mathcal{Y}_k^-(i) - \hat{\mathbf{y}}_k^-)^{\mathrm{T}} + \boldsymbol{\Sigma}_k^S \tag{25}$$

where $\mathcal{Y}_k^-(i)$ are the observations of the $i-th$ sigma-point, given through the measurement model matrix $\mathbf{h}_k$, $\boldsymbol{\Sigma}_k^S$ is the covariance matrix of measurements noise, and $\hat{\mathbf{y}}_k^-$ are the predicted observations obtained by the weighted means of the sigma-points measurements, as presented in Equations 26 and 27 [10].

$$\mathcal{Y}_k^-(i) = \mathbf{h}_k(\boldsymbol{\chi}_k^-(i)) \tag{26}$$

$$\hat{\mathbf{y}}_k^- = \sum_{i=0}^{n_{sp}-1} w_i^c \mathcal{Y}_k^-(i) \tag{27}$$

After obtaining the Kalman gain, it is possible to calculate through Equations 28 and 29, the *a posteriori* value of the covariance matrix and the state vector, which corresponds with the estimated mass and friction coefficient for the k time step.

$$\hat{\mathbf{x}}_k^+ = \hat{\mathbf{x}}_k^- + \mathbf{K}_k(\mathbf{o}_k - \hat{\mathbf{y}}_k^-) \tag{28}$$

$$\mathbf{P}_k^+ = \mathbf{P}_k^- - \mathbf{K}_k \mathbf{P}_{\mathbf{y_k y_k}} \mathbf{K}_k^{\mathrm{T}} \tag{29}$$

where $\mathbf{o}_k$ are the real sensor observations, which compared with the predicted measurements results into the filter innovation.

4.2. Error-State Extended Kalman Filter with force estimation

Once that the suspended mass of the vehicle and the friction coefficient of the tire-road contact are estimated for the time step k, it is possible to start with the estimation of the states and inputs of the vehicle through the errorEKF with force estimation. This filter is based on indirect estimation, also known as error-state estimation. It combines the efficiency of an EKF filter with the easy integration of the dynamical system in the UKF filters [28]. The multibody model runs without modifications, and hence any formulation or integrator can be employed, including methods with implicit integrators, dependent coordinates, projections, etc (see, e.g. [21]).

In previous works of the errorEKF, such as [28, 11, 12, 13], a set of dependent coordinates have been used, based on Matrix-R formulation [8]. Instead, the

model of this work is developed in independent coordinates based on a semi-recursive formulation [19]. This work highlights therefore the implementation flexibility of the errorEKF.

Following the diagram of Figure 2, for each time step, this method first runs one step of the multibody simulation, obtaining the coordinates $\mathbf{z}_{MBS}$, velocities $\dot{\mathbf{z}}_{MBS}$ and accelerations $\ddot{\mathbf{z}}_{MBS}$. For the estimation process, the state vector consists in the *error* in position, velocity and acceleration of the degrees of freedom of the mechanism. Including the accelerations on the state vector allows to estimate the inputs of the system, in a kind of unknown input observer. Thus, the state vector is,

$$\mathbf{x}^{\mathrm{T}} = \left[\Delta\mathbf{z}^{\mathrm{T}}, \Delta\dot{\mathbf{z}}^{\mathrm{T}}, \Delta\ddot{\mathbf{z}}^{\mathrm{T}}\right] \tag{30}$$

where $\Delta\mathbf{z}$, $\Delta\dot{\mathbf{z}}$, $\Delta\ddot{\mathbf{z}}$ are the errors in position, velocity and acceleration respectively, such that,

$$\mathbf{z} = \mathbf{z}_{MBS} + \Delta\mathbf{z} \tag{31}$$

$$\dot{\mathbf{z}} = \dot{\mathbf{z}}_{MBS} + \Delta\dot{\mathbf{z}} \tag{32}$$

$$\ddot{\mathbf{z}} = \ddot{\mathbf{z}}_{MBS} + \Delta\ddot{\mathbf{z}} \tag{33}$$

being $\mathbf{z}$, $\dot{\mathbf{z}}$, $\ddot{\mathbf{z}}$ the *real* positions, velocities and accelerations.

After all the information from both the sensors and the model is combined into the Kalman filter, and the multibody model state is corrected, the expected value of the errors for the next time step is null. Accordingly, the propagation phase is performed as,

$$\hat{\mathbf{x}}_k^- = \mathbf{0} \tag{34}$$

$$\mathbf{P}_k^- = \mathbf{f}_{\mathbf{x}k-1}\mathbf{P}_{k-1}^+\mathbf{f}_{\mathbf{x}k-1}^{\mathrm{T}} + \mathbf{\Sigma}^P \tag{35}$$

which are the conventional equations employed in the discrete Kalman filter [26, 29]. Using the forward Euler method for the integration of the states and a random walk for modeling the acceleration error, the Jacobian matrix of the transition model, $\mathbf{f}_\mathbf{x}$ is [13],

$$\mathbf{f}_\mathbf{x} = \left[\begin{array}{c|c|c} \mathbf{I} + \frac{1}{2}\frac{\partial\Delta\hat{\ddot{\mathbf{z}}}}{\partial\mathbf{z}}\Delta t^2 & \mathbf{I}\Delta t + \frac{1}{2}\frac{\partial\Delta\hat{\ddot{\mathbf{z}}}}{\partial\dot{\mathbf{z}}}\Delta t^2 & \frac{1}{2}\mathbf{I}\Delta t^2 \\ \hline \frac{\partial\Delta\hat{\ddot{\mathbf{z}}}}{\partial\mathbf{z}}\Delta t & \mathbf{I} + \frac{\partial\Delta\hat{\ddot{\mathbf{z}}}}{\partial\dot{\mathbf{z}}}\Delta t & \mathbf{I}\Delta t \\ \hline \mathbf{0} & \mathbf{0} & \mathbf{I} \end{array}\right] \tag{36}$$

where the terms $\frac{\partial\Delta\ddot{\mathbf{z}}}{\partial\mathbf{z}}$ and $\frac{\partial\Delta\ddot{\mathbf{z}}}{\partial\dot{\mathbf{z}}}$ account for the effect of the acceleration error through the force models of the multibody model. Since $\mathbf{z}$ are independent coordinates,

$$\frac{\partial\Delta\ddot{\mathbf{z}}}{\partial\mathbf{z}} = -\mathbf{M}^{-1}\bar{\mathbf{K}} \tag{37}$$

$$\frac{\partial\Delta\ddot{\mathbf{z}}}{\partial\dot{\mathbf{z}}} = -\mathbf{M}^{-1}\bar{\mathbf{C}} \tag{38}$$

being $\bar{\mathbf{K}}$ and $\bar{\mathbf{C}}$ the stiffness and damping matrices of the multibody model respectively, which can be derived following [30].

In order to propagate the corrections, the equations applied are similar to the equations defined in the discrete extended Kalman filter [26, 29]. Thus,

$$\mathbf{\Sigma}_k = \mathbf{h}_{\mathbf{x}k}\mathbf{P}_k^-\mathbf{h}_{\mathbf{x}k}^{\mathrm{T}} + \mathbf{\Sigma}_k^S \tag{39}$$

$$\mathbf{K}_k = \mathbf{P}_k^-\mathbf{h}_{\mathbf{x}k}^{\mathrm{T}}\mathbf{\Sigma}_k^{-1} \tag{40}$$

$$\hat{\mathbf{x}}_k^+ = \mathbf{0} + \mathbf{K}_k(\mathbf{o}_k - \mathbf{h}(\mathbf{z}_k, \dot{\mathbf{z}}_k, \ddot{\mathbf{z}}_k)) \tag{41}$$

$$\mathbf{P}_k^+ = (\mathbf{I} - \mathbf{K}_k\mathbf{h}_{\mathbf{x}k})\mathbf{P}_k^- \tag{42}$$

where the innovation covariance matrix, $\mathbf{\Sigma}_k$, represents the uncertainty in the system state projected via the sensor function, $\mathbf{h}_{\mathbf{x}k}\mathbf{P}_k^-\mathbf{h}_{\mathbf{x}k}^{\mathrm{T}}$, plus an additional Gaussian noise originated at the sensor itself, $\mathbf{\Sigma}_k^S$. Small values of $\mathbf{\Sigma}_k$ mean that the observation introduces useful information to constrain the estimation of the system state. By evaluating the Kalman gain, $\mathbf{K}_k$, the estimation of the mean and covariance are updated in Equations 41 and 42 respectively [11].

Once that the *a posteriori* state vector is known, the estimated position $\hat{\mathbf{z}}$, velocities $\hat{\dot{\mathbf{z}}}$ and accelerations $\hat{\ddot{\mathbf{z}}}$ for the time step k are also obtained through Equation 33. The new estimated values are propagated through the rest variables of the model in order to update the force models, such as springs, dampers or tires.

The error in accelerations also implies an error in the generalized forces $\Delta\mathbf{Q}$, i.e the forces that should be applied to the vehicle model to avoid the estimated acceleration error. The force increments, $\Delta\mathbf{Q}$, are given by,

$$\Delta\mathbf{Q} = \mathbf{M}\hat{\ddot{\mathbf{z}}} - \hat{\mathbf{Q}} \tag{43}$$

Thus, adding $\Delta\mathbf{Q}$ to the vector of generalized forces ensures that the forces and kinematic corrections are compatible. Applying it to the integration of the following time step, the expected acceleration error of the multibody model for the next time step is null [13]. Since the vehicle is modeled in independent coordinates, each element of $\Delta\mathbf{Q}$ corresponds to its respective variable in the set of coordinates $\mathbf{z}$ (Equation 1).

This approach assumes that the forces are acting on the degrees of freedom of the multibody model. In some mechanisms, this assumption can bring to an accurate solution. In the case of vehicle dynamics, as stated in Section 3.2, the main forces acting over the longitudinal and lateral vehicle behavior come from the tires. Applying the force increments, $\Delta\mathbf{Q}$, over the chassis could result into undesired tire reactions, which could lead to inaccurate tire forces estimations.

4.2.1. Tire Forces Distribution

In order to apply correctly the force increments, it is proposed to transform the elements of $\Delta\mathbf{Q}$ related to the chassis into tire forces increments, as illustrated in Figure 3.

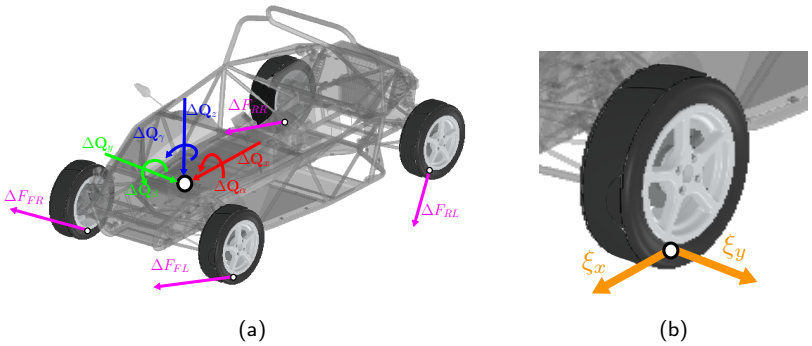


Fig. 3 Mapping to the tires of the forces increment applied in the chassis by the errorEKF.

However, there are multiple tire forces combinations which can produce the desired effects on the chassis. In this work, the selected criteria is to minimize the tire forces increments. This leads to a least square problem such as,

$$\mathbf{\Delta F}_{FL} + \mathbf{\Delta F}_{FR} + \mathbf{\Delta F}_{RL} + \mathbf{\Delta F}_{RR} = \Delta \mathbf{Q}_{xyz} \tag{44}$$

$$\mathbf{r}_{FL} \times \mathbf{\Delta F}_{FL} + \mathbf{r}_{FR} \times \mathbf{\Delta F}_{FR} + \mathbf{r}_{RL} \times \mathbf{\Delta F}_{RL} + \mathbf{r}_{RR} \times \mathbf{\Delta F}_{RR} = \Delta \mathbf{Q}_{\alpha\beta\gamma} \tag{45}$$

where $\mathbf{\Delta F}$ is the tire force increment, $\mathbf{r}$ is the contact point between the wheel and the road, and FL, FR, RL, RR refer to the front left, front right, rear left and rear right wheels respectively.

Since the tire forces are related to the tire deformation (Equations 14, 15, 16), it is required to transform tire forces increments obtained into tire deformations. Projecting each $\mathbf{\Delta F}$ over the tire axis, shown in Figure 3b, results in the required increments on longitudinal and lateral tire forces for correcting the longitudinal and lateral dynamic states of the vehicle. Considering that the tire deformation, ξ, is linear,

$$\hat{\xi}_x = \xi_x + \frac{\Delta F_x}{k_x} \tag{46}$$

$$\hat{\xi}_y = \xi_y + \frac{\Delta F_y}{k_y} \tag{47}$$

As a last step, the force models of the vehicle are updated with the estimated tire states. Since some terms of $\Delta \mathbf{Q}$ have been derived into tire forces, the final correction in forces is obtained after subtracting the resulting tire forces. The terms related to the longitudinal and lateral displacements, as well as the yaw, are almost null since they have been derived to the tires deformation.

5. Measurement noise, covariance matrices of the plant and sensor models

When working with Kalman filters, there are several types of uncertainties that must be considered. For instance, the sensors employed in the measure-

ments are not perfect, which leads to the existence of noise. In addition, there are always unknown modeling errors.

The measurement noise and the covariance matrices of the plant are the parameters where all the uncertainties explained above are included. The importance of the covariance matrices is such that if they are not properly set, the filter can become unstable [13].

5.1. Measurement noise

The noise of the sensors is perfectly determined in the simulation environment. A common procedure, followed in this work, consists in generating it from a multibody model which acts as the real system. Later, white Gaussian noise is generated and added to the sensors signal, fulfilling the assumptions of Kalman filtering [26]. When using real sensors, although they are not perfect, the noise is usually provided by the manufacturer and can be considered as white Gaussian noise.

5.2. Covariance matrices

In the case of the plant noise, the errors of the multibody model with respect to real system cannot be identified as most of them are unknown. Accordingly, the plant noise properties must be tuned in order to reach a robust solution which converges to accurate solutions independently of the model errors. In addition, as reflected in [26], if fictitious plant noise is added, the filter will place more emphasis on the measurements instead of on the inaccurate model, thus improving filter performance. As a counterpart, in case the system model is correct, this will reduce the performance. Thus, the covariance matrix of the plant noise should be tuned to balance the performance and accuracy of the filter.

The structure of the covariance matrix for the UKF is presented in Equation 48. It is a diagonal matrix with the tuned noises, σ, for the mass and the friction coefficient as elements.

$$\mathbf{\Sigma}^P_{UKF} = \begin{bmatrix} \sigma_m^2 & 0 \\ 0 & \sigma_\mu^2 \end{bmatrix} \tag{48}$$

For the errorEKF with force estimation, the structure of the plant matrix is as proposed in [29]. The structure of the covariance matrix for the plant noise can be obtained from the transition matrix given by the equation (36) yielding,

$$\mathbf{\Sigma}^P_{errorEKF} = \sigma^2 \begin{bmatrix} \frac{\Delta t^5}{20} & \frac{\Delta t^4}{8} & \frac{\Delta t^3}{6} \\ \frac{\Delta t^4}{8} & \frac{\Delta t^3}{3} & \frac{\Delta t^2}{2} \\ \frac{\Delta t^3}{6} & \frac{\Delta t^2}{2} & \Delta t \end{bmatrix} \tag{49}$$

where σ^2 is a diagonal matrix which contains the noises of each multibody variable presented in the state vector from Equation 30. It must be noted that only the constant elements of the transition matrix were considered. Thus, the process noise matrix is constant during the simulation and it can be evaluated before the simulation starts [13], reducing the computational cost of the observer.

5.3. Sensor models

The sensors employed in this work vary from position sensors, as the ones for measuring the suspension deflection, to angular velocity sensors, such as the gyroscope, and acceleration sensors. The models of the sensors have been developed from the set of independent variables which define the vehicle model (Equation 1), and are grouped into the term $\mathbf{h}(\mathbf{z}, \dot{\mathbf{z}}, \ddot{\mathbf{z}})$. The expressions for the observations of each sensor can be found in [11, 13]. The Jacobian matrix of the measurements $\mathbf{h_x}$ required by the errorEKF is obtained as,

$$\mathbf{h_x} = \begin{bmatrix} \mathbf{h_z} & \mathbf{h_{\dot{z}}} & \mathbf{h_{\ddot{z}}} \end{bmatrix} \tag{50}$$

$$\mathbf{h_z} = \frac{\partial \mathbf{h}(\mathbf{z}, \dot{\mathbf{z}}, \ddot{\mathbf{z}})}{\partial \mathbf{z}} \qquad \mathbf{h_{\dot{z}}} = \frac{\partial \mathbf{h}(\mathbf{z}, \dot{\mathbf{z}}, \ddot{\mathbf{z}})}{\partial \dot{\mathbf{z}}} \qquad \mathbf{h_{\ddot{z}}} = \frac{\partial \mathbf{h}(\mathbf{z}, \dot{\mathbf{z}}, \ddot{\mathbf{z}})}{\partial \ddot{\mathbf{z}}} \tag{51}$$

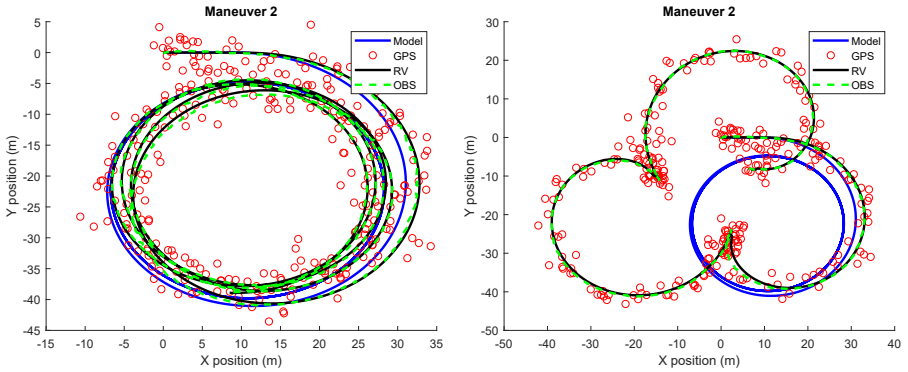
6. Results and discussion

In this section, the performance of the state-parameter-input observer presented during Section 4 is tested over different maneuvers and the accuracy of the estimations is discussed. The vehicle model variables estimated by the *observer* are compared with their respective values in the *real vehicle*. This allows a clear understanding of the *model* drift corrections done by the *observer* versus the *real vehicle* behavior.

The first maneuver consists in a turn with a constant steering angle and throttle position on a flat road. As stated in Section 2, errors in the vehicle's mass and friction coefficient are introduced. First, in *Maneuver 1*, the *real vehicle* has a mass of 600 kg and a friction coefficient of 0.8, while the *model* has a mass of 700 kg and a friction coefficient of 1. Next, in order to test a more aggressive maneuver, called *Maneuver 2*, the friction coefficient of the *real vehicle* is reduced to 0.6, in such a way that the vehicle skids in every turn. The drift existing between the *real vehicle* and the *model* can be seen in Figure 4. Only the first 60 seconds of the maneuver are shown for clarity of the figures.

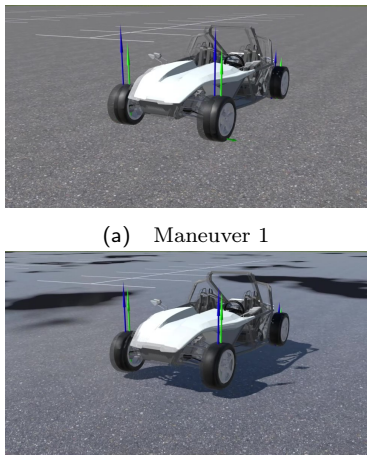
For *Maneuver 2* (Figure 4b), the trajectories of the vehicle are totally different than from *Maneuver 1*. While the *model* performs concentric circles, the *real vehicle* is not able to follow the same trajectory due to its lower tire-road friction coefficient. In every turn, the tire-road friction coefficient is too low to counteract the tangential forces. This causes the vehicle to skid in a turn of 180° and to loose velocity. In spite of the huge differences in the trajectories, the *observer* corrects the *model* drift and tracks the path of the *real vehicle* for both maneuvers.

For more clarity, the maneuvers can be seen in the videos of Figure 5. The *real vehicle* is represented as the opaque vehicle, while the *observer* is the semi-transparent vehicle. It can be appreciated in both videos how the corrections are applied to the *observer*, so that it can track the *real vehicle* during the maneuver. The tire forces of each vehicle are also represented in the videos as arrows pointing on the direction of the force.



(a) *Maneuver 1* (b) *Maneuver 2*

Fig. 4 Trajectories of the turning maneuvers performed to test the state-parameter-input observer. The abbreviations *RV* and *OBS* are referred to *real vehicle* and *observer* positions respectively.



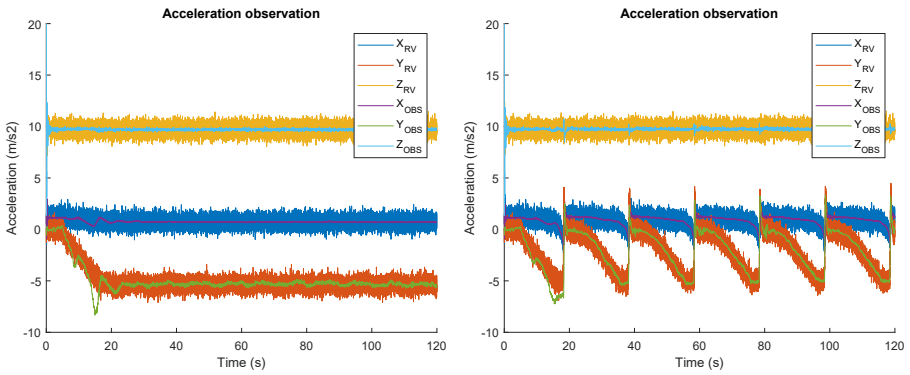
(a) Maneuver 1

(b) Maneuver 2

Fig. 5 Maneuvers performed by the *real vehicle* (opaque) and *observer* (semi-transparent). The green arrows represent the tire forces acting on the *real vehicle*. The blue arrows represent the tire forces acting on the *observer*.

Concerning the rest of the estimations, the measurements gathered from the *observer* show the same trend than the one of the sensor measurements provided by the *real vehicle*. Moreover, the noise of the estimated measurements is reduced with respect to the sensor data employed to feed the *observer*. Figure 6 shows such noise reduction for the vehicle acceleration. After an initial phase of stabilization, the accuracy of the estimated accelerations increases. The effects of the different tire-road friction coefficients can be noticed by comparing the measurements of both maneuvers. Although the dynamics of each maneuvers

are quite different, the state-parameter-input observer is able to correct the drift between the *real vehicle* and the *model* in both cases.



(a) *Maneuver 1* (b) *Maneuver 2*

Fig. 6 Vehicle accelerations for *Maneuvers 1* and *2*. The subscripts *RV* and *OBS* refer to *real vehicle* and *observer* accelerations respectively.

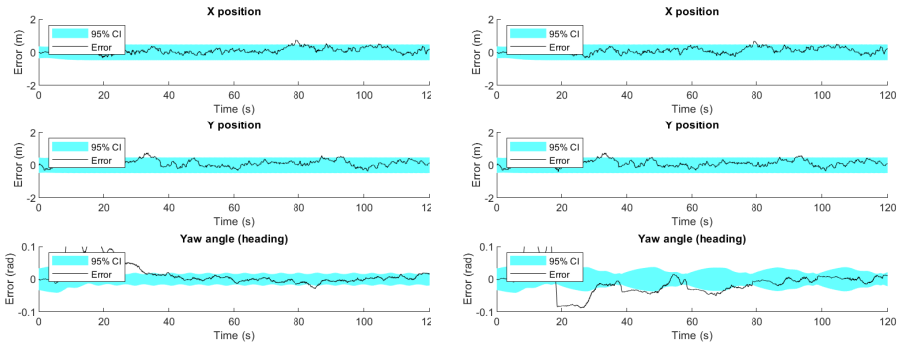
The errors in the estimations are shown from a quantitative point of view in Table 2. The root-mean square error (RMSE) was used to compare the predicted values with the real ones thus giving a better insight on the estimations accuracy. The predictions derived from the state-parameter-input observer (SPI) are compared with the respective predictions obtained from the errorEKF only.

Table 2 RMSE in the estimated positions and accelerations by the state-parameter-input observer compared with the errorEKF estimations and the real sensor measurements.

RMSE: Position and accelerations					
Magnitude	Sensor	*Maneuver 1*		*Maneuver 2*	
		SPI	errorEKF	SPI	errorEKF
Position (m)	1.9075	0.2202	0.1988	0.2107	0.4023
X accel. (m/s^2)	0.4492	0.0326	0.1319	0.0461	0.3018
Y accel. (m/s^2)	0.447	0.1473	0.7923	0.2014	1.5429
Z accel. (m/s^2)	0.4485	0.0783	0.3496	0.0860	0.3662

Both estimators are able to predict the position of the vehicle with much less error than the GPS. Regarding the accelerations, the errorEKF shows more deviation in the lateral acceleration than the accelerometer with respect to its real value. This difference is higher in the *Maneuver 2*, due to the effects of skidding. However, when the errorEKF is combined with the parameter estimation in the state-parameter-input observer, the error in the accelerations is strongly reduced and produces highly precise acceleration measurements.

In Figure 7, the confidence intervals for the position and heading of the chassis in each maneuver are shown. This variables are also of interest, since they are related with the navigation of the vehicle. The confidence interval gives a different insight on the error of the estimations. It is based on the diagonal elements of the covariance matrix of the plant noise of the system (Section 5). In Figures 7a and 7b, the error is represented for a confidence interval of 95%.



(a) *Maneuver 1* (b) *Maneuver 2*

Fig. 7 Navigation variables for *Maneuvers 1* and *2*. The subscripts *RV* and *OBS* refer to *real vehicle* and *observer* accelerations respectively.

Regarding *Maneuver 1*, except for an initial phase of initialization, the error in the position and heading is within the band of the 95% confidence interval. This means that only the 5% of these estimations will have an error higher than 1.96 times the standard deviation of the variable. With respect to *Maneuver 2*, the error in position is inside the limits of the confidence interval during the maneuver. However, regarding the heading, it tends to be out of bounds during a period of time right after the vehicle skids. This behaviour is mitigated at the end of the simulation. It should be noted how, especially in the case of the heading, the filter changes the value of the covariance (and thus its confidence on the model) in order to correct the existent drift.

In addition, the covariance matrix can be used as an indicator of the system's observability. As shown in Figure 7, the covariance of the position and heading are stable during the maneuver. This trend is repeated through the rest of elements of the covariance matrix. If the system were not observable, it could be expected an unlimited growth of the covariance of the states.

However, the main interest lies in predicting variables that are difficult or costly to measure. That is the case for the tire forces. In Figures 8 and 9, the estimated tire forces for the rear-right (RR) wheel are compared with the respective values for the *real vehicle* and for the *model*. The RMSE is also evaluated for the tire forces in order to show the improvements resulting from the parameter estimation. The RMSE with respect to the *real vehicle* are shown

in Table 3

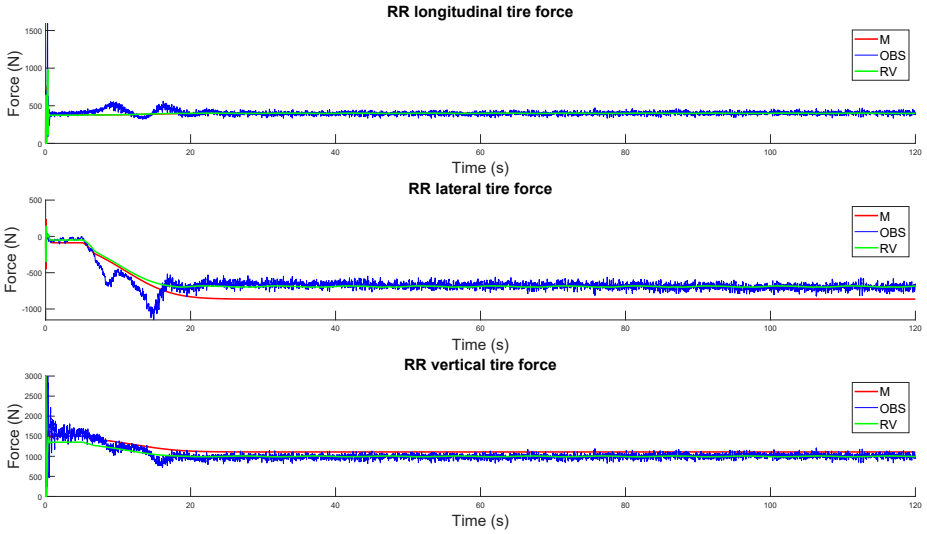


Fig. 8 Tire forces of the rear-right wheel during *Maneuver 1*. The abbreviations *RV* and *OBS* are referred to *real vehicle* and *observer* forces respectively.

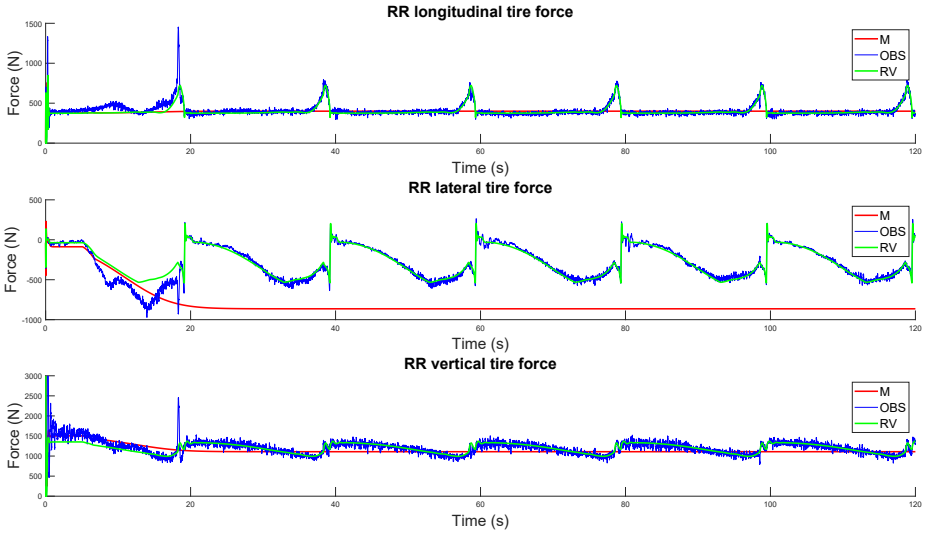


Fig. 9 Tire forces of the rear-right wheel during *Maneuver 2*. The abbreviations RV and OBS are referred to *real vehicle* and *observer* forces respectively.

Table 3 RMSE in the estimated tire forces by the state-parameter-input observer compared with the errorEKF estimations.

RMSE: Tire forces				
Magnitude	*Maneuver 1*		*Maneuver 2*	
	SPI	errorEKF	SPI	errorEKF
RR long. tire force (N)	19.23	76.09	21.51	165.32
RR lat. tire force (N)	39.96	237.69	28.17	265.58
RR vert. tire force (N)	51.55	144.25	60.48	180.09

From the RMSE, it can be seen how the parameter estimations reduces the error in the tire forces estimation. It is more noticeable in the lateral tire force estimation, since its value is affected by both the mass and the tire-road friction coefficient. For both maneuvers, after an initial phase of stabilization, the estimated tire forces track with accuracy the real values.

The improvements in the estimations are due to the combined use of the errorEKF and the UKF for parameter estimation. The predictions for the mass and tire-road friction coefficient are presented in Figure 10.

It can be seen that, as in the previous estimations, there is a delay until the parameters are correctly estimated. Regarding *Maneuver 1*, the estimations of both parameters is smooth (Figures 10a and 10c). Meanwhile, in *Maneuver 2*, the estimation of the parameters has more noise (Figures 10b and 10d). In *Maneuver 2*, the behaviour of the *real vehicle* and the *model* is quite different, and the state-parameter-input observer has to apply strong corrections. As a consequence, it is more difficult for the observer to track the *real* value of the parameters. This kind of effects can be mitigated through the covariance matrices of the system (Section 5). However, in this work, these matrices are adjusted based on a trial-error procedure. Thus, it is difficult to achieve an optimal configuration. It is expected that an improvement in the tuning procedure would lead to an improvement of the estimations.

6.1. Computational cost

To maximally extend the applicability of the proposed state-parameter-input observer to the vehicle dynamics field, it should be possible to execute the *observer* in three different models: offline, live and real-time. As a consequence, the computational complexity of the *observer* should allow to run it in real-time on modern hardware. Although this work is focused on obtaining accurate estimations, a few observations related to computational cost are given hereafter.

When combining the errorEKF with the UKF for parameter estimation, the computational cost increases. This issue should be considered when implementing the observer on hardware devices with lower performance such as the ones found in-vehicle (modern ECUs or on-board data acquisition systems), in which the errorEKF has already been executed in real-time [31]. The simulation times taken by each of the observers tested in this work are presented in Table 4. The simulations are executed in a single core of a PC with an Intel Core i5 at 3.50

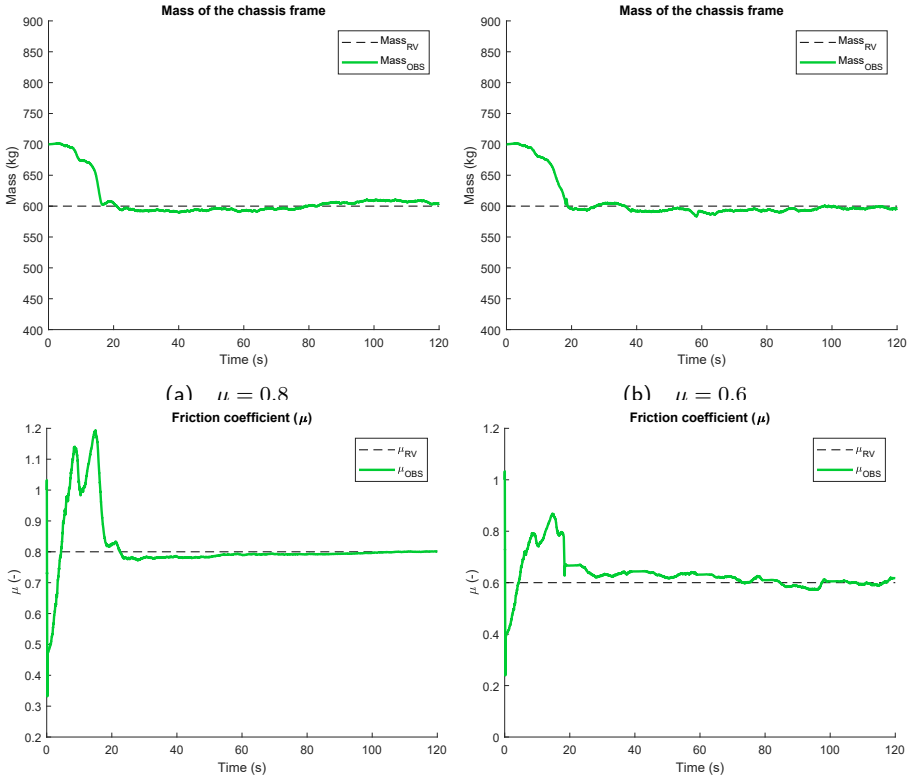


Fig. 10 Parameter estimation in the turning maneuvers performed to test the state-parameter-input observer. The subscripts RV and OBS refer to *real vehicle* and *observer* values respectively.

GHz and 8 Gb of RAM. As shown in Table 4, using this particular hardware, the state-parameter-input observer is about 4 times slower than the errorEKF.

Table 4 Summary of the computational cost of each observer

Computational Cost				
Version	Sim. Time (s)	Δt (s)	Comp. Time (s)	Real-time ratio
errorEKF	60	0.004	7.18	8.36
SPI	60	0.004	29.35	2.04

565

6.2. Discussion

Based on the results obtained in this research, it was demonstrated that combining the errorEKF with a parameter estimator significantly increases the

accuracy of the estimations. The proposed state-parameter-input observer has shown to provide accurate predictions even for aggressive maneuvers in which the vehicle looses traction and skids.

Regarding the estimated variable nature, the error on the position of the vehicle, it is lower by one order of magnitude than for the GPS signal employed for the corrections. For the accelerations of the chassis frame, the proposed observer improves the measurements from the accelerometer. The estimations show less error and noise than the sensor data fed to the observer for the corrections. This behavior is appreciated in the other measurements: GPS speed, angular velocities, suspension displacements and wheel angles.

For the tire forces estimation, complementing the errorEKF with the parameter estimation results in an error reduction from almost 50% to around 9% in the case of the lateral forces for the *Maneuver 2*. For the longitudinal and vertical tire forces, the error is reduced from 41% and 18% to 5% respectively.

7. Conclusions and future work

Virtual sensors provide additional information from a system, offering better insight in its behavior. In vehicle dynamics applications, variables such as tire forces are of high interest. However, the sensors available in the market for measuring them are costly and, therefore, is only employed on particular tests during the design phase.

With the objective of providing accurate virtual sensors for vehicle dynamics, the multibody simulation approach can be used. With this approach, a vehicle can be modeled with a high level of detail. Hence, virtual dynamics sensors can be used during vehicle engineering analysis, testing and troubleshooting. Unlike analytical modeling methods, multibody modeling methods permit taking into account non-linearities occurring for example during severe maneuvers. In addition, more virtual sensors are available when using multibody models. As a counterpart, this approach is limited by the high computational cost associated to multibody simulations and the need for more information and parameters from the vehicle.

In [13], an efficient state observer referred as errorEKF showed promising results when applied to a multibody model of a planar mechanism. The errorEKF improved the performance of existing filters based on multibody models. In [11], the errorEKF is combined with a full multibody model of a vehicle achieving real-time execution in a PC. Due to its computational efficiency, the errorEKF can be suitable for real-time automotive applications. However, the force estimations were not as accurate as expected.

In order to improve the estimations, a new observer is designed in this work combining the errorEKF with a UKF for parameter estimation. Uncertain parameters, such as the mass of the vehicle (which varies with passengers or luggage) and the tire-road friction coefficient (which is affected by meteorological conditions, type of road or tire state), are estimated thus leading to a better accuracy. Results show that the estimated tire forces reduce the error in approximately 41%. Other variables, such as the position or the accelerations,

show that the observer is able to provide estimations with less error and noise than the respective physical sensors and the respective virtual sensors from the errorEKF.

In future works, the state-parameter-input observer presented should be implemented in a real scenario. The computational performance of the observer can be improved if the UKF is replaced by an EKF. The main limitation is the Jacobian matrix of the parameters with respect to the multibody variables. Different ways to numerically compute the Jacobian matrix could be explored. Also, the tuning of the covariance matrix is a difficult process, full of uncertainties. Furthermore, the covariance matrix of the plant noise should be tailored if the maneuver changes significantly. Due to the strong influence of this covariance matrix in the estimations, its tuning process should be further explored.

Acknowledgements

This work has been partially financed by the Spanish Ministry of Economy and Competitiveness (MINECO) and EU-ERDF funds under the project 'Observadores de estados y entradas basados en modelos multicuerpo detallados aplicados al control de vehículos' (TRA2014-59435-P) and through the grant BES-2015-071372.

References

[1] World Health Organization, Global status report on road safety 2018 (2018).

[2] B. L. Boada, M. J. Boada, V. Diaz, Vehicle sideslip angle measurement based on sensor data fusion using an integrated ANFIS and an Unscented Kalman Filter algorithm, Mechanical Systems and Signal Processing 72-73 (2016) 832–845. doi:10.1016/j.ymssp.2015.11.003.

[3] G. Reina, M. Paiano, J.-L. Blanco-Claraco, Vehicle parameter estimation using a model-based estimator, Mechanical Systems and Signal Processing 87 (2017) 227–241. doi:10.1016/j.ymssp.2016.06.038.
URL https://linkinghub.elsevier.com/retrieve/pii/S0888327016302205

[4] B. L. Boada, M. J. L. Boada, H. Zhang, Sensor Fusion Based on a Dual Kalman Filter for Estimation of Road Irregularities and Vehicle Mass Under Static and Dynamic Conditions, IEEE/ASME Trans. Mechatron. 24 (3) (2019) 1075–1086. doi:10.1109/TMECH.2019.2909977.
URL https://ieeexplore.ieee.org/document/8684917/

[5] M. Acosta, A. Alatorre, S. Kanarachos, A. Victorino, A. Charara, Estimation of tire forces, road grade, and road bank angle using tire model-less approaches and Fuzzy Logic., IFAC-PapersOnLine 50 (1) (2017) 14836–14842. doi:10.1016/j.ifacol.2017.08.2583.

URL https://linkinghub.elsevier.com/retrieve/pii/S2405896317335127

[6] A. J. Rodríguez, R. Pastorino, A. Carro-Lagoa, K. Janssens, M. A. Naya, Hardware acceleration of multibody simulations for real-time embedded applications, Multibody Syst Dyn (Apr. 2020). doi:10.1007/s11044-020-09738-w.
URL https://doi.org/10.1007/s11044-020-09738-w

[7] J. Cuadrado, D. Dopico, A. Barreiro, E. Delgado, Real-time state observers based on multibody models and the extended Kalman filter, Journal of Mechanical Science and Technology 23 (4) (2009) 894–900.

[8] J. G. d. Jalon, E. Bayo, Kinematic and Dynamic Simulation of Multibody Systems: The Real-Time Challenge, Springer Science & Business Media, 2012, google-Books-ID: ye_SBwAAQBAJ.

[9] J. Cuadrado, D. Dopico, J. A. Perez, R. Pastorino, Automotive observers based on multibody models and the extended Kalman filter, Multibody System Dynamics 27 (1) (2012) 3–19.

[10] R. Pastorino, D. Richiedei, J. Cuadrado, A. Trevisani, State estimation using multibody models and non-linear Kalman filter, International Journal of Non-Linear Mechanics 53 (2013) 83–90.

[11] E. Sanjurjo, State observers based on detailed multibody models applied to an automobile, Phd. thesis, University of A Coruña (2016).
URL http://hdl.handle.net/2183/17963

[12] E. Sanjurjo, M. Á. Naya, J. L. Blanco-Claraco, J. L. Torres-Moreno, A. Giménez-Fernández, Accuracy and efficiency comparison of various nonlinear Kalman filters applied to multibody models, Nonlinear Dynamics (feb 2017). doi:10.1007/s11071-017-3354-z.

[13] E. Sanjurjo, D. Dopico, A. Luaces, M. A. Naya, State and force observers based on multibody models and the indirect Kalman filter, Mechanical Systems and Signal Processing 106 (2018) 210–228.
URL https://doi.org/10.1016/j.ymssp.2017.12.041

[14] I. Palomba, D. Richiedei, A. Trevisani, Kinematic state estimation for rigid-link multibody systems by means of nonlinear constraint equations, Multibody System Dynamics (2016) 1–22.

[15] I. Palomba, D. Richiedei, A. Trevisani, E. Sanjurjo, A. Luaces, J. Cuadrado, Estimation of the digging and payload forces in excavators by means of state observers, Mechanical Systems and Signal Processing 134 (2019) 106356. doi:10.1016/j.ymssp.2019.106356.
URL http://www.sciencedirect.com/science/article/pii/S0888327019305771

[16] T. A. Wenzel, K. J. Burnham, M. V. Blundell, R. A. Williams, Dual extended Kalman filter for vehicle state and parameter estimation, Vehicle System Dynamics 44 (2) (2006) 153–171. doi:10.1080/00423110500385949.
URL http://www.tandfonline.com/doi/abs/10.1080/00423110500385949

[17] C. Zong, D. Hu, H. Zheng, Dual extended Kalman filter for combined estimation of vehicle state and road friction, Chin. J. Mech. Eng. 26 (2) (2013) 313–324. doi:10.3901/CJME.2013.02.313.
URL http://link.springer.com/10.3901/CJME.2013.02.313

[18] J. Cuadrado, D. Vilela, I. Iglesias, A. Martín, A. Peña, A Multibody Model to Assess the Effect of Automotive Motor In-wheel Configuration on Vehicle Stability and Comfort, in: Proceedings of the ECCOMAS Thematic Conference on Multibody Dynamics 2013, Multibody Dynamics 2013, Zagreb, Croatia, 2013, p. 10.

[19] J. Cuadrado, D. Dopico, M. Á. Naya Villaverde, Penalty, semi-recursive and hybrid methods for MBS real-time dynamics in the context of structural integrators, Multibody System Dynamics 12 (2) (2004) 117–132.

[20] D. Dopico, Formulaciones semi-recursivas y de penalización para la dinámica en tiempo real de sistemas multicuerpo, Ph.D. thesis, Universidade da Coruña (2004).

[21] J. Cuadrado, D. Dopico, M. Á. Naya Villaverde, M. González, Real-Time Multibody Dynamics and Applications, in: Simulation Techniques for Applied Dynamics, no. 507, 2008, pp. 247–311. doi:10.1007/978-3-211-89548-1_6.

[22] E. Kuiper, J. J. M. Van Oosten, The PAC2002 advanced handling tire model, Vehicle System Dynamics 45 (sup1) (2007) 153–167. doi:10.1080/00423110701773893.
URL http://www.tandfonline.com/doi/abs/10.1080/00423110701773893

[23] D. Dopico, A. Luaces, M. Gonzalez, J. Cuadrado, Dealing with multiple contacts in a human-in-the-loop application, Multibody Syst Dyn 25 (2) (2011) 167–183. doi:10.1007/s11044-010-9230-y.
URL http://link.springer.com/10.1007/s11044-010-9230-y

[24] W. Hirschberg, G. Rill, H. Weinfurter, Tire model TMeasy, Vehicle System Dynamics 45 (sup1) (2007) 101–119. doi:10.1080/00423110701776284.
URL http://www.tandfonline.com/doi/abs/10.1080/00423110701776284

[25] K. Bogdanski, M. C. Best, Kalman and particle filtering methods for full vehicle and tyre identification, Vehicle System Dynamics 56 (5) (2018)

769–790. doi:10.1080/00423114.2017.1337914.
URL https://www.tandfonline.com/doi/full/10.1080/00423114.2017.1337914

[26] D. Simon, Optimal State Estimation: Kalman, H Infinity, and Nonlinear Approaches, Wiley, Hoboken, 2006.

[27] S. J. Julier, J. K. Uhlmann, New extension of the Kalman filter to nonlinear systems, in: I. Kadar (Ed.), Signal Processing, Sensor Fusion, and Target Recognition VI, Vol. 3068, International Society for Optics and Photonics, SPIE, 1997, pp. 182 – 193. doi:10.1117/12.280797.
URL https://doi.org/10.1117/12.280797

[28] E. Sanjurjo, J. L. Blanco, J. L. Torres, M. A. Naya, Testing the efficiency and accuracy of multibody-based state observers, in: ECCOMAS Thematic Conference on Multibody Dynamics, Barcelona, 2015, pp. 1595–1606.

[29] M. Grewal, A. Andrews, Kalman filtering: theory and practice using MATLAB®, Wiley, New Jersey, 2008.

[30] D. Dopico, Y. Zhu, A. Sandu, C. Sandu, Direct and Adjoint Sensitivity Analysis of Ordinary Differential Equation Multibody Formulations, Journal of Computational and Nonlinear Dynamics 10 (1) (2014) 011012.

[31] A. J. Rodríguez, R. Pastorino, E. Sanjurjo, A. Luaces, M. A. Naya, Implementación de Observador de Estados basado en Modelos Multicuerpo en Tiempo real en Plataformas Embebidas, in: Proceedings of Congreso Nacional de Ingeniería Mecánica, Madrid, Spain, 2018, p. 7.